

# D’ARTAGNAN: Counterfactual Video Generation

Hadrien Reynaud<sup>1</sup>, Athanasios Vlontzos<sup>1</sup>, Mischa Dombrowski<sup>2</sup>, Ciarán Lee<sup>3,4</sup>,  
Arian Beqiri<sup>5,6</sup>, Paul Leeson<sup>5,7</sup>, and Bernhard Kainz<sup>1,2</sup>

<sup>1</sup> Department of Computing, Imperial College London, London, UK  
`hadrien.reynaud19@imperial.ac.uk`

<sup>2</sup> Friedrich–Alexander University Erlangen–Nürnberg, DE  
<sup>3</sup> Spotify

<sup>4</sup> University College London, London, UK  
<sup>5</sup> Ultromics Ltd, Oxford, UK

<sup>6</sup> King’s College London, School of Biomedical Engineering & Imaging Sciences,  
London, UK

<sup>7</sup> John Radcliffe Hospital, Cardiovascular Clinical Research Facility, Oxford, UK

**Abstract.** Causally-enabled machine learning frameworks could help clinicians to identify the best course of treatments by answering counterfactual questions. We explore this path for the case of echocardiograms by looking into the variation of the Left Ventricle Ejection Fraction, the most essential clinical metric gained from these examinations. We combine deep neural networks, twin causal networks and generative adversarial methods for the first time to build D’ARTAGNAN (Deep ARTificial Twin-Architecture GeNeRAtive Networks), a novel *causal* generative model. We demonstrate the soundness of our approach on a synthetic dataset before applying it to cardiac ultrasound videos by answering the question: "What would this echocardiogram look like if the patient had a different ejection fraction?". To do so, we generate new ultrasound videos, retaining the video style and anatomy of the original patient, with variations of the Ejection Fraction conditioned on a given input. We achieve an SSIM score of 0.79 and an R2 score of 0.51 on the counterfactual videos. Code and models are available at: [anonymous].

**Keywords:** Causal Inference · Twin Networks · Counterfactual Image Generation

## 1 Introduction

How would this patient’s scans look like if they had a different Left Ventricular Ejection Fraction (LVEF)? How would this Ultrasound (US) view appear if I turned the probe by 5 degrees? These are important causality related questions that physicians and operators ask explicitly or implicitly during the course of an examination in order to reason about the possible pathologies of the patient. While in the second case the interventional query of turning the probe is easy to resolve – by performing the action– queries like the first case, where we ask a

counterfactual question, cannot be answered that easily. Indeed, these fall under the third and highest rung of Pearl’s [24] hierarchy of causation.

Counterfactual queries probe into alternative scenarios that might have occurred had our actions been different. For the first question of this paper, we ask ourselves how the patients scans would look like if they had a different LVEF. Here, the treatment would be the different ejection fraction, and the outcome, the different set of scans. Note that this is a query that is *counter-to* our observed knowledge that the patients scans exhibited a specific LVEF. As such, standard Bayesian Inference that conditions on the observed data without any further considerations is not able to answer this type of questions.

**Contributions:** In this paper (1) We extend the causal inference methodology known as Deep Twin Networks [32] into a novel generative modelling method (Deep ARtificial Twin-Architecture GeNerAtive Networks (D’ARTAGNAN) <sup>1</sup>) able to handle counterfactual queries. To the best of our knowledge, this is the first time such an approach is explored for medical image analysis and computer vision. (2) We apply our framework on the synthetic MorphoMNIST [7] and real-world EchoNet-Dynamic [22] datasets, exhibiting that our method can perform well in both, fully controlled environments, and on real medical cases.

**Related works:** Generating synthetic US images can be performed with physics-based simulators [27,8,11,16,19,12,6] and other techniques, like registration-based methods [17]. However, these methods are usually very computationally expensive and do not generate fully realistic images. With the shift into deep learning, Generative Adversarial Network (GAN)-based techniques have emerged. They can be based on simulated US priors or other imaging modalities (MRI, CT) [9,28,29,2,1,30] to condition the anatomy of the generated US images. Our method uses real cardiac US to condition the generation of new US with modified LVEF, thus differentiating itself from previous works. Furthermore, recently there has been much interest in using machine learning to estimate interventional conditional distributions [33,15,18,3]. However, comparatively fewer works focus on the counterfactual query estimation. [23,20] abide by the Abduction-Action-Prediction paradigm and use deep neural networks for the abduction step, which, however, is computationally very expensive. [10] derive a parametric mathematical model for the estimation of one of the probabilities of causation, while [32] use [4] to develop deep twin networks.

## 2 Preliminaries

**Structural causal models** We work in the Structural Causal Models (SCM) framework. Chapter 7 of [24] gives an in-depth discussion. For an up-to-date, review of counterfactual inference and Pearl’s Causal Hierarchy, see [5].

**Definition 1 (Structural Causal Model)** *A structural causal model (SCM) specifies a set of latent variables  $U = \{u_1, \dots, u_n\}$  distributed as  $P(U)$ , a set of observable variables  $= \{v_1, \dots, v_m\}$ , a directed acyclic graph (DAG), called the*

<sup>1</sup> D’Artagnan is the fourth Musketeer from the French tale “The three Musketeers”.

causal structure of the model, whose nodes are the variables  $U \cup V$ , a collection of functions  $F = \{f_1, \dots, f_n\}$ , such that  $v_i = f_i(PA_i, u_i)$ , for  $i = 1, \dots, n$ , where  $PA$  denotes the parent observed nodes of an observed variable.

The collection of functions  $F$  and the distribution over latent variables induces a distribution over observable variables:  $P(V = v) := \sum_{\{u_i | f_i(PA_i, u_i) = v_i\}} P(u_i)$ . In this manner, we can assign uncertainty over observable variables despite the fact that the underlying dynamics are deterministic. Furthermore, the *do*-operator forces variables to take certain values, regardless of the original causal mechanism. Graphically,  $do(X = x)$  means deleting edges incoming to  $X$  and setting  $X = x$ . Probabilities involving  $do(x)$  are normal probabilities in submodel  $M_x$ :  $P(Y = y | do(X = x)) = P_{M_x}(y)$ .

**Counterfactual inference** The latent distribution  $P(U)$  allows to define probabilities of counterfactual queries,  $P(Y_y = y) = \sum_{u | Y_x(u) = y} P(u)$ . For  $x \neq x'$  one can also define joint counterfactual probabilities,  $P(Y_x = y, Y_{x'} = y') = \sum_{u | Y_x(u) = y, \& Y_{x'}(u) = y'} P(u)$ . Moreover, one can define a counterfactual distribution given seemingly contradictory evidence. Given a set of observed evidence variables  $E$ , consider the probability  $P(Y_x = y' | E = e)$ .

**Definition 2 (Counterfactual)** *The counterfactual sentence “ $Y$  would be  $y$  (in situation  $U = u$ ), had  $X$  been  $x$ ”, denoted  $Y_x(u) = y$ , corresponds to  $Y = y$  in submodel  $M_x$  for  $U = u$ .*

Despite the fact that Def. 2 may involve interventions that contradict the evidence, it is well-defined, as the intervention specifies a new submodel. Indeed,  $P(Y_x = y' | E = e)$  is given by [24] as  $\sum_u P(Y_x(u) = y') P(u|e)$ .

As opposed to the standard *Abduction-Action-Prediction* paradigm, we will be operating under the Twin Model methodology. Originally proposed by Balke and Pearl in [4], this method allows efficient counterfactual inference as a feed forward Bayesian process. It has also been shown empirically in [14] to offer computational savings relative to abduction-action-prediction. A twin network consists of two interlinked networks, one representing the real world and the other the counterfactual world being queried. Constructing a twin network given a structural causal model and using it to compute a counterfactual query is as follows: First, one duplicates the given causal model, denoting nodes in the duplicated model via superscript  $*$ . Let  $V = \{v_1, \dots, v_n\}$  be observable nodes in the causal model and  $V^* = \{v_1^*, \dots, v_n^*\}$  the duplication of these. Then, for every node  $v_i^*$  in the duplicated, or “counterfactual” model, its latent parent  $u_i^*$  is replaced with the original latent parent  $u_i$  in the original, or “factual”, model, such that the original latent variables are now a parent of two nodes,  $v_i$  and  $v_i^*$ . The two graphs are linked only by common latent parents, but share the same node structure and generating mechanisms. To compute a general counterfactual query  $P(Y = y | E = e, do(X = x))$ , one modifies the structure of the counterfactual network by dropping arrows from parents of  $X^*$  and setting them to value  $X^* = x$ . Then, in the twin network with this modified structure, one computes the probability  $P(Y^* = y | E = e, X^* = x)$  via standard Bayesian inference techniques, where  $E$  are factual nodes.

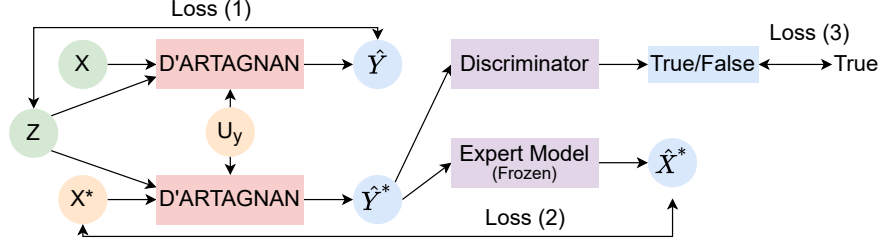


Fig. 1: Framework around D’ARTAGNAN. The green variables are known, the orange are sampled from distributions and the blue are generated by deep neural networks. We enumerate the three losses we use to train the framework.

### 3 Method

**Deep Twin Networks** The methodology we propose is based on Deep Twin Networks. The training procedure and parametrization are borrowed from [32], who presents a causal framework. The information flow we implement to build our Twin Network follows this causal framework to implement our own Twin Network. To define a generative deep twin network, we note our factual and counterfactual treatments (inputs unique to each branch),  $X$  and  $X^*$ . The confounder (input shared by both branches) is noted  $Z$ . A Deep Twin Network serves as a base for the proposed methodology. In order to implement Deep Twin Networks, we borrow the parametrization and training procedure from [32]. We maintain the interdependencies of the variables of the causal graph by ensuring the information paths of our network directly mimic the graphical structure of a Twin Network. For the purposes of using a twin network in our generative pipeline we define the treatments  $X, X^*$  to be the treatments of our factual and counterfactual queries, the confounder  $Z$  represents the auxiliary information regarding the images, for example the dimensions or label of depicted elements. The factual and counterfactual outcomes  $\hat{Y}, \hat{Y}^*$  are considered either as latent embeddings used in conjunction with a decoding network, or as target image or video. Training such a model thus requires well-defined treatments and confounders, as well as counterfactual label  $Y^*$  and an estimate of the unobserved parameters  $U_Y$ .

Following the methodology of [32,26] one could employ propensity score matching to augment our dataset in such a way that supervised training of the counterfactual head is possible. However, in the case of synthetic examples this is not necessary as we have access to the ground truth counterfactual. For our real world data, we do not possess expressive enough covariates to enable high quality propensity score matching, and it is not possible to retrieve real labels for both the factual and counterfactual. Hence, we identify three qualities we want our network to possess when generating counterfactual videos that can help train our method: (1) produce a factual and counterfactual output that will share general visual features, such as style and anatomy. (2) produce accurate

factual and counterfactual videos with respect to the intervened upon variable, and (3) the counterfactual videos are visually indistinguishable from a real one that possess the intervened upon features.

First, to resolve feature (1) we share the weights of the branches in the network, such that we train a single branch on two tasks in parallel. Then by training the factual branch to produce the ground truth videos, given their LVEF as treatment and entire video as confounder, the network learns to retain the style and anatomical structure of the echocardiogram in the confounder. We signify this by *Loss 1* in Figure 1 mathematically defined as an L1 loss. Secondly, for feature (2) we pre-train an expert network to regress the treatment values. The expert network takes a video as input and outputs the estimated LVEF. The expert network weights’ are frozen when training the Twin model and the difference between the expert network prediction and the counterfactual treatment denotes *Loss 2* in Figure 1 again parametrized as an L1 loss. Finally, feature (3) calls for the well-known GAN framework, where we train a neural network to discriminate between real and fake images or videos, while training the Twin Network. This constitutes an adversarial *Loss 3*. With those 3 losses, we can train D’ARTAGNAN to produce pairs of visually accurate and anatomically matching videos with given LVEFs.

To learn the distribution of  $U_Y$ , we follow [13,32] and without loss of generality we can write  $Y = f(X, Z, g(U'_Y))$  with  $U'_Y \sim \mathcal{E}$  and  $U_Y = g(U'_Y)$ , where  $\mathcal{E}$  is some easy-to-sample-from distribution, such as a Gaussian or Uniform. Effectively, we cast the problem of determining  $U_Y$  to learning the appropriate transformation from  $\mathcal{E}$  to  $U_Y$ . For ease of understanding, we will be using  $U_Y$  henceforth to signify our approximation  $g(U'_Y)$  of the true unobserved parameter  $U_Y$ . In addition to specifying the causal structure, the following standard assumptions are needed to correctly estimate  $\mathbb{E}(Y|do(X), Z)$  [26]: 1) *Ignorability*: there are no unmeasured confounders; 2) *Overlap*: every unit has non-zero probability of receiving all treatments given their observed covariates.

## 4 Experimentation

**Datasets** As part of our evaluation we use two publicly available datasets, a synthetic version of MorphoMNIST [7] and the clinical Echonet-Dynamic [22] dataset. MorphoMNIST enables fine-grained perturbations of the MNIST digits through morphological functions (thinning, thickening, swelling and fracture), as well as measurement of the digits in terms of area, length, thickness, slant, width and height. We generate a dataset of 2.4 million images, split randomly into training and validation sets (80% / 20%). For each original image  $I_i$ , we sample 40 perturbation vectors  $p_{i,j}$  with random parameters for the five possible perturbations including the identity, with which we generate images  $I_{p_{i,j}}$ . We also measure the original digits to produce vectors  $m_i$  and one-hot encode the digits’ label into vectors  $l_i$ . To complete the dataset, we pre-train a Vector Quantized-Variational AutoEncoder (VQ-VAE) model to encode all  $I_{p_{i,j}}$  into latent embeddings  $\mathcal{H}_{i,j}$ .

The clinical dataset Echonet-Dynamic [22] consists of 10,030 4-chamber echocardiography videos with  $112 \times 112$  pixels resolution and various length, frame rates, image quality and cardiac conditions. Each video contains a pair of consecutive labelled End-Systolic (ES) and End-Diastolic (ED) frames. Each video also comes with a clinically measured LVEF. For our use case, we greyscale and re-sample all the videos to 64 frames, with a frame rate of 32 images per second. All videos shorter than 2s are discarded. We make sure to keep the two labelled frames in the sampled frames. For the resulting 9724 videos dataset, the original split is kept, with 7227 training, 1264 validation and 1233 testing images.

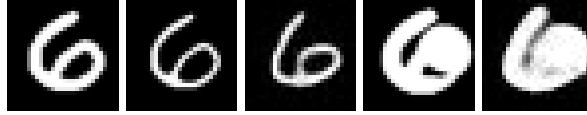


Fig. 2: Left to right: original image, ground truth factual image, predicted factual image, ground truth counterfactual image, predicted counterfactual image. Factual perturbation is Thinning, Counterfactual perturbation is Thickening and Swelling.

**MorphoMNIST** For the purposes of our synthetic experiment, we define a deep twin network as in [32].  $X$  and  $X^*$  are the factual and counterfactual treatments,  $Z$  is the confounder,  $U_Y$  is the noise and  $Y$  and  $Y^*$  are the outcome labels. For each original image, we set  $Z_i = [l_i, m_i]$  to contain the one-hot encoded labels as well as the measurement of the original image, and we sample two perturbations vectors  $p_{i,m}$  and  $p_{i,n}$  and their corresponding latent embeddings  $\mathcal{H}_{i,m}$  and  $\mathcal{H}_{i,n}$ , where  $n, m \in \llbracket 0, 40 \rrbracket$ ,  $n \neq m$ . We set  $X = p_{i,m}$ ,  $X^* = p_{i,n}$ ,  $Y = \mathcal{H}_{i,m}$  and  $Y^* = \mathcal{H}_{i,n}$ . We sample  $U_Y \sim [\mathcal{N}(0, 0.25) \bmod 1 + 1]$  and disturb the output of the neural network that combines  $X, X^*$  and  $Z$  by multiplying it with  $U_Y$ . This ensures that the network cannot easily disentangle the noise, as it would be the case with a concatenation.

In order to simplify the problem at hand we train a VQ-VAE [21] to embed our high dimensional frames into a smaller dimensionality distilled embedding. The VQ-VAE is trained first to project inputs to a latent space  $\mathcal{H} \in \mathbb{R}^{(q \times h \times w)}$  and reconstruct them. Once trained, the VQ-VAE weights are frozen. The produced latent embeddings are used as the targets  $(Y, Y^*)$  for the Deep Twin Network. The Deep Twin Network is therefore trained to produce latent embeddings, which can then be decoded to reconstruct the represented images, using the pre-trained VQ-VAE decoder.

We assess the quality of the results by three means: (1) *Embeddings' MSE*: We sample a quintuplet  $(Z, X, X^*, Y, Y^*)$  and 1000  $U_Y$ . The MSE between all  $\hat{Y}_i$  and  $Y$  are computed and used to order the pairs  $(\hat{Y}_i, \hat{Y}_i^*)$  in ascending order. We keep the sample with the lowest MSE as our factual estimate and compute the MSE between  $\hat{Y}_0^*$  and  $Y^*$  to get our counterfactual MSE score. (2) *SSIM*: We use the Structural SIMilarity metric between the perturbed images  $I_{gt} = I_{p_{i,j}}$ , the

images reconstructed by the VQVAE  $I_{rec}$  and the images reconstructed from the latent embedding produced by the twin network  $I_{pred}$  to get a quantitative score over the images. (3) *Images*: We sample some images to qualitatively assess best and worst cases scenarios for this framework. We show the quantitative results in Table 1(a), and qualitative results in Figure 2 and in the appendix.

Table 1: Metrics for MorphoMNIST (a) and EchoNet-Dynamic (b) experiments.

Metric	Factual Counterfactual		Metric	Factual Counterf.	
$MSE(Y, \hat{Y})$	2.3030	2.4232	R2	0.87	0.51
$SSIM(I_{gt}, I_{rec})^\dagger$	0.9308	0.9308	MAE	2.79	15.7
$SSIM(I_{rec}, I_{pred})$	0.6759	0.6759	RMSE	4.45	18.4
$SSIM(I_{gt}, I_{pred})$	0.6707	0.6705	SSIM	0.82	0.79

(a) MSE and SSIM scores.  $^\dagger$ No ordering is performed (b) D’ARTAGNAN LVEF and re-construction metrics.

**Echonet Dynamic** As stated in Section 3, part of our methodology requires an **Expert Model** that will be able to regress the LVEF from videos similar to what our model will be outputting. To do so, we re-implement the ResNet 2+1D network [31] as it was shown to be the best option for LVEF regression in [22]. We opt not to use transformers as they do not supersede convolutions for managing the temporal dimension, as shown in [25]. We purposefully keep the size of this model as low as possible in order to minimize its memory footprint, as it will be operating together with the D’ARTAGNAN model and a frame discriminator. The weights of the expert network are frozen after this point and thus not updated while D’ARTAGNAN is training. Metrics for this model are presented in the Appendix.

**D’ARTAGNAN** We implement the D’ARTAGNAN framework described in Section 3. The backbone of each branch is a custom-made Conv2+1D [31] network with residual connections. At each training step, we sample a video ( $V_i$ ) and LVEF ( $\psi_i$ ). We set our factual treatment  $X = \psi_i$  and our counterfactual treatment to a value sampled from a uniform distribution in range 0-1, at least 10% away from  $X$ . The confounder is set to  $Z = V_i$  and the noise  $U_Y \sim [\mathcal{N}(0, 0.25) \bmod 1 + 1]$  is concatenated with the feature maps in the middle of the network.

**Discriminator** We build a custom discriminator architecture using five “residual multiscale convolutional blocks”, with kernel sizes 3, 5, 7 and appropriate padding at each step, followed by a max-pooling layer. Using multiscale blocks enables the discriminator to look both at local and global features. This is extremely important in US images because of the noise in the data, that needs to be both ignored, for anatomical identification, and accounted for to ensure that counterfactual US images look real. We test this discriminator both as a frame-based discriminator and a video-based discriminator, by changing the 2D layers to 3D layers where appropriate. We note that, given our architecture, the

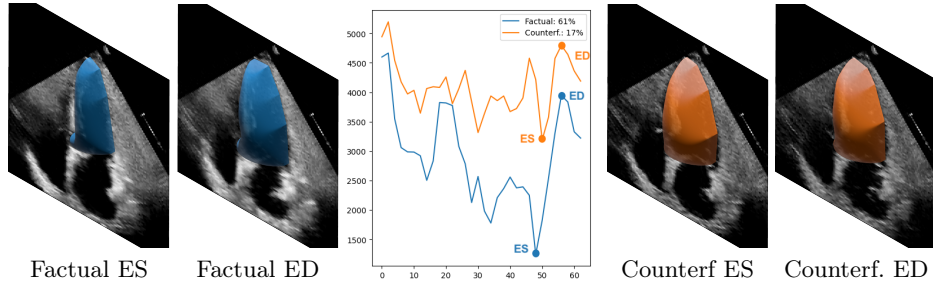


Fig. 3: Qualitative results for D’ARTAGNAN over the same confounder and noise. Left: factual ES and ED frames. Middle: left ventricle area over time, obtained with a segmentation network as in [22]. Dots represent where the corresponding frames were sampled. Right: counterfactual ES and ED frames. Anatomy is preserved across videos, while the LVEF fraction is different. The volume representation is drawn over a predicted segmentation.

3D version of the model requires slightly less memory but double the processing power compared to the 2D model.

**Training the framework** The discriminator is trained using the  $\hat{Y}^*$  as fake examples and the real videos  $V$  as real examples. To ensure that the networks converge, we make sure that the three L1 losses are on the same scale. The discriminator is trained with a fixed learning rate, but when used to train D’ARTAGNAN, it is weighted by a sigmoid function offset by 3 epochs. In the 3 initial epochs, the discriminator loss will have little impact on D’ARTAGNAN. We apply the same strategy to the expert model loss, but we offset it by 5 epochs. By offsetting the losses, we ensure that the network first learns to reconstruct the factual outcome, thus maintaining the anatomy and style. By doing so, we drastically increase the speed at which the network is capable of outputting realistic-looking videos, thus speeding up the training of the discriminator that starts seeing accurate fake videos much quicker. Once the discriminator and D’ARTAGNAN are capable of generating and discriminating realistic-looking videos, the expert network loss is activated and forces the generator to take into account the counterfactual treatment, while the factual treatment is enforced by the reconstruction loss. The losses are also scaled, such that the discriminator loss has a relative weight of 3 compared to the reconstruction and expert loss.

**Metrics** As D’ARTAGNAN acts as a GAN generator, there is no simple metric to evaluate it quantitatively. We decide to compare the treatment LVEF and the regressed LVEF for the produced video as a regression problem using the R2, MAE and RMSE scores over the best videos. To obtain the best video, we sample 100  $U_Y$  noise samples and keep the videos where the MAE is the lowest. In order to evaluate how the anatomy is preserved, we compute the SSIM over the best video and input video for all videos. Results are shown in Table 1b.

**Qualitative** In Figure 3 we show video frame examples to showcase the quality of the reconstructed frames, as well as how the anatomy and style are maintained.



**Discussion** The predicted LVEF has an MAE of 15.7% which is not optimal. This can come from many factors like the use of the same dataset to train the Expert model and D'ARTAGNAN, the limited number of real videos, or the limited size of the networks due to the necessity of working with three models at once. Those problems can be addressed with hyperparameter search over larger models, as well as additional medical data.

## 5 Conclusion

In this paper we introduce D'ARTAGNAN, a Deep Twin Generative Network able to produce counterfactual images and videos. We showcase its performance in both synthetic and real world medical datasets and achieve visually accurate results and high quantitative scores. In future works, we could explore other treatments, as changing the heartbeat, as well as less constrained confounders, like image segmentations.

**Acknowledgements:** This work was supported by Ultromics Ltd., the UKRI Centre for Doctoral Training in Artificial Intelligence for Healthcare (EP/S023283/1), and the UK Research and Innovation London Medical Imaging and Artificial Intelligence Centre for Value Based Healthcare. We thank the NVIDIA corporation for their GPU donations used in this work.

## References

1. Abbasi-Sureshjani, S., Amirrajab, S., Lorenz, C., Weese, J., Pluim, J., Breeuwer, M.: 4d semantic cardiac magnetic resonance image synthesis on xcat anatomical model (2 2020), <http://arxiv.org/abs/2002.07089>
2. Amirrajab, S., Abbasi-Sureshjani, S., Khalil, Y.A., Lorenz, C., Weese, J., Pluim, J., Breeuwer, M.: Xcat-gan for synthesizing 3d consistent labeled cardiac mr images on anatomically variable xcat phantoms (7 2020), <http://arxiv.org/abs/2007.13408>
3. Assaad, S., Zeng, S., Tao, C., Datta, S., Mehta, N., Henao, R., Li, F., Duke, L.C.: Counterfactual representation learning with balancing weights. In: International Conference on Artificial Intelligence and Statistics. pp. 1972–1980. PMLR (2021)
4. Balke, A., Pearl, J.: Probabilistic evaluation of counterfactual queries. In: AAAI (1994)
5. Bareinboim, E., Correa, J.D., Ibeling, D., Icard, T.: On pearl’s hierarchy and the foundations of causal inference. Tech. rep., Columbia University, Stanford University (2020)
6. Burger, B., Bettinghausen, S., Radle, M., Hesser, J.: Real-time gpu-based ultrasound simulation using deformable mesh models. *IEEE transactions on medical imaging* **32**(3), 609–618 (2012)
7. Castro, D.C., Tan, J., Kainz, B., Konukoglu, E., Glocker, B.: Morpho-MNIST: Quantitative assessment and diagnostics for representation learning. *Journal of Machine Learning Research* **20**(178) (2019)

8. Cong, W., Yang, J., Liu, Y., Wang, Y.: Fast and automatic ultrasound simulation from ct images. *Computational and mathematical methods in medicine* **2013** (2013)
9. Cronin, N.J., Finni, T., Seynnes, O.: Using deep learning to generate synthetic b-mode musculoskeletal ultrasound images. *Computer Methods and Programs in Biomedicine* **196**, 105583 (2020). <https://doi.org/https://doi.org/10.1016/j.cmpb.2020.105583>, <https://www.sciencedirect.com/science/article/pii/S0169260720314164>
10. Cuellar, M., Kennedy, E.H.: A non-parametric projection-based estimator for the probability of causation, with application to water sanitation in kenya. *Journal of the Royal Statistical Society: Series A (Statistics in Society)* **183**(4), 1793–1818 (2020)
11. Dillenseger, J.L., Laguitton, S., Éric Delabrousse: Fast simulation of ultrasound images from a ct volume. *Computers in Biology and Medicine* **39**, 180–186 (2009). <https://doi.org/10.1016/j.combiomed.2008.12.009>
12. Gao, H., Choi, H.F., Claus, P., Boonen, S., Jaecques, S., Lenthe, G.H.V., Perre, G.V.D., Lauriks, W., D’Hooge, J.: A fast convolution-based methodology to simulate 2-dd/3-d cardiac ultrasound images. *IEEE Transactions on Ultrasonics, Ferroelectrics, and Frequency Control* **56**, 404–409 (2 2009). <https://doi.org/10.1109/TUFFC.2009.1051>
13. Goudet, O., Kalainathan, D., Caillou, P., Lopez-Paz, D., Guyon, I., Sebag, M., Tritas, A., Tubaro, P.: Learning functional causal models with generative neural networks. *arXiv preprint arXiv:1709.05321* (2017)
14. Graham, L., Lee, C.M., Perov, Y.: Copy, paste, infer: A robust analysis of twin networks for counterfactual inference. *NeurIPS Causal ML workshop 2019*, (2019)
15. Kocaoglu, M., Snyder, C., Dimakis, A.G., Vishwanath, S.: Causalgan: Learning causal implicit generative models with adversarial training. In: *International Conference on Learning Representations* (2018)
16. Kutter, O., Shams, R., Navab, N.: Visualization and gpu-accelerated simulation of medical ultrasound from ct images. *Computer Methods and Programs in Biomedicine* **94**, 250–266 (6 2009). <https://doi.org/10.1016/j.cmpb.2008.12.011>
17. Ledesma-Carbayo, M.J., Kybic, J., Desco, M., Santos, A., Suhling, M., Hunziker, P., Unser, M.: Spatio-temporal nonrigid registration for ultrasound cardiac motion estimation. *IEEE transactions on medical imaging* **24**(9), 1113–1126 (2005)
18. Louizos, C., Shalit, U., Mooij, J., Sontag, D., Zemel, R., Welling, M.: Causal effect inference with deep latent-variable models. In: *Proceedings of the 31st International Conference on Neural Information Processing Systems*. pp. 6449–6459 (2017)
19. Mattausch, O., Makhinya, M., Goksel, O.: Realistic ultrasound simulation of complex surface models using interactive monte-carlo path tracing (2014)
20. Oberst, M., Sontag, D.: Counterfactual off-policy evaluation with gumbel-max structural causal models. In: *International Conference on Machine Learning*. pp. 4881–4890. PMLR (2019)
21. Oord, A.v.d., Vinyals, O., Kavukcuoglu, K.: Neural discrete representation learning. *arXiv preprint arXiv:1711.00937* (2017)
22. Ouyang, D., He, B., Ghorbani, A., Yuan, N., Ebinger, J., Langlotz, C.P., Heidenreich, P.A., Harrington, R.A., Liang, D.H., Ashley, E.A., Zou, J.Y.: Video-based ai for beat-to-beat assessment of cardiac function. *Nature* **580**, 252–256 (4 2020)
23. Pawlowski, N., Castro, D.C., Glocker, B.: Deep structural causal models for tractable counterfactual inference. *arXiv preprint arXiv:2006.06485* (2020)

24. Pearl, J.: *Causality* (2nd edition). Cambridge University Press (2009)
25. Reynaud, H., Vlontzos, A., Hou, B., Beqiri, A., Leeson, P., Kainz, B.: Ultrasound video transformers for cardiac ejection fraction estimation. In: MICCAI. pp. 495–505. Springer (2021)
26. Schwab, P., Linhardt, L., Karlen, W.: Perfect match: A simple method for learning representations for counterfactual inference with neural networks. arXiv preprint arXiv:1810.00656 (2018)
27. Shams, R., Hartley, R., Navab, N.: Real-time simulation of medical ultrasound from ct images. In: International Conference on Medical Image Computing and Computer-Assisted Intervention. pp. 734–741. Springer (2008)
28. Teng, L., Fu, Z., Yao, Y.: Interactive translation in echocardiography training system with enhanced cycle-gan. *IEEE Access* **8**, 106147–106156 (2020). <https://doi.org/10.1109/ACCESS.2020.3000666>
29. Tiago, C., Gilbert, A., Snare, S.R., Sprem, J., McLeod, K.: Generation of 3d cardiovascular ultrasound labeled data via deep learning (2021)
30. Tomar, D., Zhang, L., Portenier, T., Goksel, O.: Content-preserving unpaired translation from simulated to realistic ultrasound images (3 2021), <http://arxiv.org/abs/2103.05745>
31. Tran, D., Wang, H., Torresani, L., Ray, J., LeCun, Y., Paluri, M.: A closer look at spatiotemporal convolutions for action recognition. In: Proceedings of the IEEE conference on Computer Vision and Pattern Recognition. pp. 6450–6459 (2018)
32. Vlontzos, A., Kainz, B., Gilligan-Lee, C.M.: Estimating the probabilities of causation via deep monotonic twin networks. arXiv preprint arXiv:2109.01904 (2021)
33. Yoon, J., Jordon, J., Van Der Schaar, M.: Ganite: Estimation of individualized treatment effects using generative adversarial nets. In: International Conference on Learning Representations (2018)